Journal of Vacuum Science and Technology A

RESEARCH ARTICLE | JUNE 06 2023

Effect of drift layer doping and NiO parameters in achieving 8.9 kV breakdown in 100 μm diameter and 4 kV/4 A in 1 mm diameter NiO/β-Ga_2O_3 rectifiers

Special Collection: Gallium Oxide Materials and Devices

Jian-Sian Li ; Chao-Ching Chiang ; Xinyi Xia ; Hsiao-Hsuan Wan ; Fan Ren ; S. J. Pearton

J. Vac. Sci. Technol. A 41, 043404 (2023)
https://doi.org/10.1116/6.0002722

JVST A
Journal of Vacuum Science & Technology A

ARTICLE

avs.scitation.org/journal/jva

Effect of drift layer doping and NiO parameters in achieving 8.9 kV breakdown in 100 μm diameter and 4 kV/4 A in 1 mm diameter NiO/β-Ga_2O_3 rectifiers

Cite as: J. Vac. Sci. Technol. A **41**, 043404 (2023); doi: 10.1116/6.0002722
Submitted: 25 March 2023 · Accepted: 11 May 2023 ·
Published Online: 6 June 2023

Jian-Sian Li,[1] Chao-Ching Chiang,[1] Xinyi Xia,[1] Hsiao-Hsuan Wan,[1] Fan Ren,[1] and S. J. Pearton[2,a)]

AFFILIATIONS

[1]Department of Chemical Engineering, University of Florida, Gainesville, Florida 32606
[2]Department of Materials Science and Engineering, University of Florida, Gainesville, Florida 32606

Note: This paper is part of the Special Topic Collection on Gallium Oxide Materials and Devices.
[a)]**Electronic mail:** spear@mse.ufl.edu

ABSTRACT

The effect of doping in the drift layer and the thickness and extent of extension beyond the cathode contact of a NiO bilayer in vertical NiO/β-Ga_2O_3 rectifiers is reported. Decreasing the drift layer doping from 8×10^{15} to 6.7×10^{15} cm^{-3} produced an increase in reverse breakdown voltage (V_B) from 7.7 to 8.9 kV, the highest reported to date for small diameter devices (100 μm). Increasing the bottom NiO layer from 10 to 20 nm did not affect the forward current–voltage characteristics but did reduce reverse leakage current for wider guard rings and reduced the reverse recovery switching time. The NiO extension beyond the cathode metal to form guard rings had only a slight effect (~5%) in reverse breakdown voltage. The use of NiO to form a pn heterojunction made a huge improvement in V_B compared to conventional Schottky rectifiers, where the breakdown voltage was ~1 kV. The on-state resistance (R_{ON}) was increased from 7.1 m Ω cm^2 in Schottky rectifiers fabricated on the same wafer to 7.9 m Ω cm^2 in heterojunctions. The maximum power figure of merit $(V_B)^2/R_{ON}$ was 10.2 GW cm^{-2} for the 100 μm NiO/Ga_2O_3 devices. We also fabricated large area (1 mm^2) devices on the same wafer, achieving V_B of 4 kV and 4.1 A forward current. The figure-of-merit was 9 GW cm^{-2} for these devices. These parameters are the highest reported for large area Ga_2O_3 rectifiers. Both the small area and large area devices have performance exceeding the unipolar power device performance of both SiC and GaN.

I. INTRODUCTION

The increasing electrification of automobiles and the need to switch renewable energy sources in the existing power grid has increased demand for energy efficient power electronica capable of higher voltage and currents than existing Si devices. This has focused attention on the wide and ultra-wide bandgap semiconductors,[1–5] with the latter including diamond, AlN, and Ga_2O_3. The ability to grow large diameter, high quality crystals from melt-grown methods and the attendant low cost of production has spurred interest in β-Ga_2O_3.[1–5] One of the goals is to achieve a high-power figure of merit for power electronic devices, defined as $(V_B)^2/R_{ON}$ where V_B is the reverse breakdown voltage and R_{ON} is the on-state resistance.[1,3,4] To achieve a high-power figure of merit, a rectifier must have a low drift layer concentration, with high electron mobility, as well as low R_{ON}, and optimized edge termination to prevent current crowding.[1,5–21] The breakdown voltage is larger for thicker drift layers, but this degrades on-resistance. To achieve a low Ron, a thin drift layer with high electron mobility is required. In addition, vertical geometry devices are desirable, because of their higher power conversion efficiency and absolute currents compared to lateral devices.[1,3–5] Power rectifiers are also building blocks for many advanced power handling systems.

A drawback with Ga_2O_3 is the absence of facile p-type doping. All of the potential acceptor dopants have large ionization energies

and are not significantly ionized at room temperature. This has led to the use of p-type oxides, principally polycrystalline NiO, to form p-n heterojunctions with n-type Ga_2O_3.[6–14] The forward current transport mechanism in such junctions is typically recombination at low biases and trap-assisted tunneling at higher bias.[10,21–26] Promising rectifier performance has been reported with this approach,[12–14,21–39] including V_B of 8.32 kV, with figure of merit of 13.2 GW cm^{-2}.[12]

Optimization of the heterojunction rectifier device structure is crucial to achieve both high V_B and low R_{ON}, as well as providing management of the maximum electric fields within the structure to enhance further the device voltage blocking capability.[40–46] The design variables include the thickness and doping of the layers, doping in the drift layer and the use of the NiO as a guard ring by extending it beyond the metal cathode. In this paper, we report an investigation of the effect of these parameters on the performance of NiO/Ga_2O_3 vertical rectifiers. A new highest V_B for these devices is achieved.

II. EXPERIMENT

We made both vertical geometry Schottky rectifiers and NiO/Ga_2O_3 rectifiers on the same wafers. The parameters investigated are shown in the schematic of the vertical heterojunction rectifiers in Fig. 1. We varied the thickness of the second layer in the bilayer NiO (10 or 20 nm, with fixed thickness of the top layer held constant at 10 nm) and the length of the NiO extension beyond the cathode contact (12–20 μm) to form guard rings. The choice of these parameters was guided by TCAD simulations with the Silvaco Atlas code of electric field distributions, as reported previously.[14] Finally, we had two different drift region doping levels at a fixed thickness of 10 μm. The epitaxial layers were grown by halide vapor phase epitaxy (HVPE) on a (001) Sn-doped (10^{19} cm^{-3}) β-Ga_2O_3 single crystal substrate. These samples were purchased from Novel Crystal Technology, Japan.

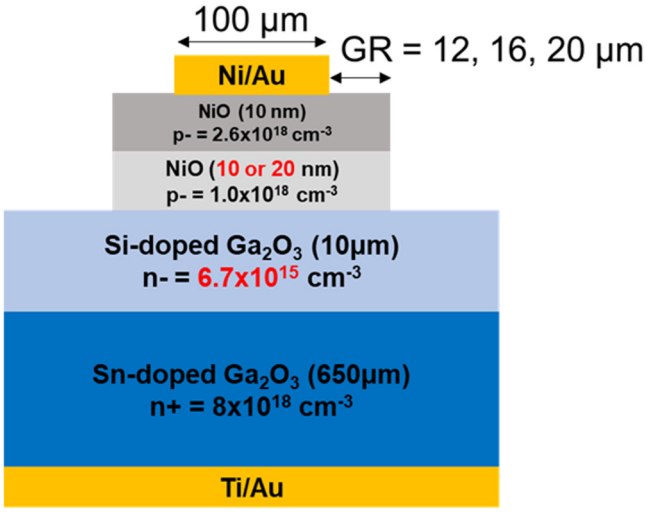

FIG. 1. Schematic of the NiO/Ga_2O_3 heterojunction rectifier. The extension of NiO beyond the Ni/Au contact to act as a guard ring was investigated for different extension lengths, as well as the thickness of the bottom NiO layer and the drift layer doping.

Ohmic contacts were made to the rear surface using a Ti/Au metal stack deposited by e-beam evaporation. This was annealed at 550 °C for 180 s under N_2. The front surface was exposed to UV/ozone exposure for 15 min to remove contamination. The NiO bilayer was deposited by rf (13.56 MHz) magnetron sputtering at a working pressure of 3 mTorr.[14,40] The hole concentration in these films was adjusted using the Ar/O_2 ratio. The structure was then annealed at 300 °C under O_2. Finally, a cathode contact of 20/80 nm Ni/Au (100 μm diameter) was deposited onto the NiO layer. The NiO was extended from 12 to 20 μm beyond the contact metal to form a guard ring. Figure 2 shows the C^{-2}–V plots for the two different drift layer doping levels. These show the carrier concentrations were 6.7×10^{15} and 8×10^{15} cm^{-3}, respectively.

The current density–voltage (J–V) characteristics were measured on a Tektronix 370-A curve tracer, 371-B curve and Agilent 4156C. For the highest reverse voltages, a Glassman power supply was employed. The reverse breakdown voltage was defined as the bias for a reverse current reaching 0.1 A–cm^2. The high bias measurements were performed in Fluorinert atmosphere at 25 °C. The devices did not suffer permanent damage at this condition but increasing the voltage a further 50–200 V led to permanent failure through breakdown at the contact periphery. The on-resistance values were calculated assuming the current spreading length is 10 μm and a 45° spreading angle. We also subtracted the resistance of the cable, probe, and chuck, which was around 10 Ω.

III. RESULTS AND DISCUSSION

A. Small area rectifiers to achieve high breakdown voltage

Figure 3 shows the forward current densities and R_{ON} values for rectifiers with different guard ring dimensions fabricated with

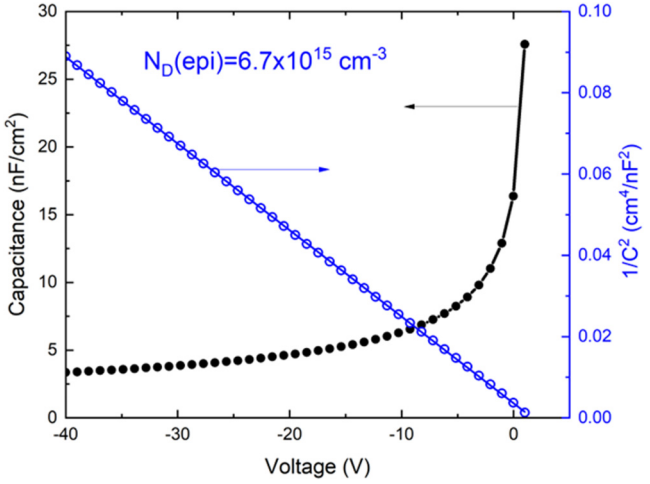

FIG. 2. C-V characteristics for determining carrier density in the drift region for the two different types of wafers investigated. The drift layer thickness was ~10 μm in both cases.

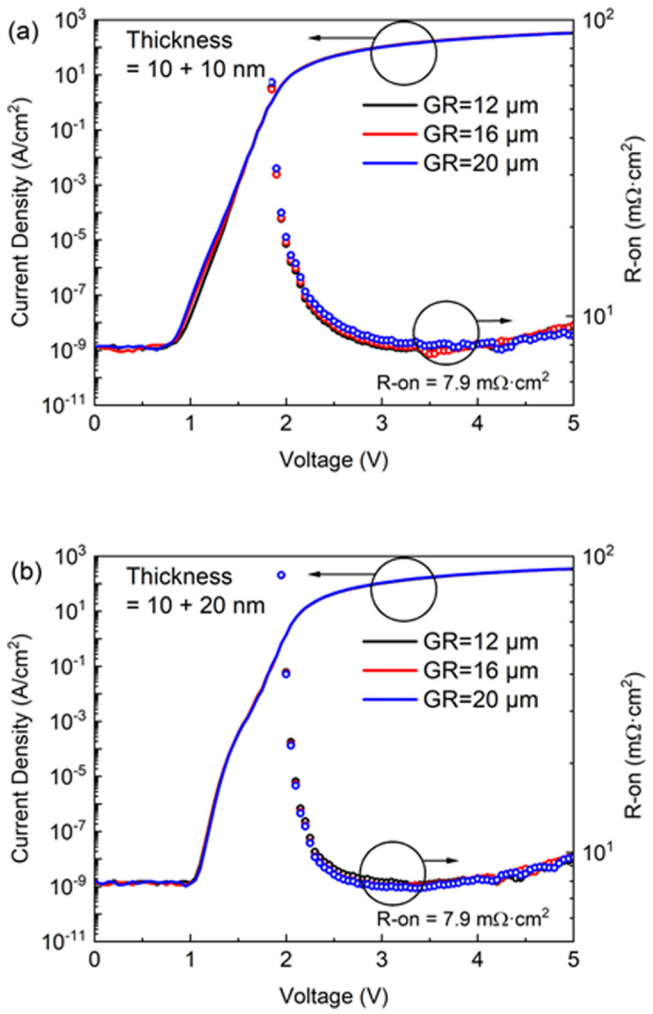

FIG. 3. Forward current densities and R_{ON} values for rectifiers with different guard rings dimensions fabricated with (a) 10/10 nm NiO bilayer or (b) 10/20 nm NiO bilayer.

(a) 10/10 nm NiO bilayer or (b) 10/20 nm NiO bilayer. These were fabricated on the drift region with the lower carrier density. There is very little difference in these forward current density characteristics for either the NO bilayer thickness or the guard ring diameter.

Figure 4 shows a comparison of the results from the NiO/Ga_2O_3 heterojunction rectifiers with the Schottky rectifier fabricated on the same wafer. The on-resistance for the former was 7.9 mΩ cm^{-2}. For the Schottky rectifiers, this parameter was slightly lower, as expected, at 7.1 mΩ cm^2. Both types of devices had forward current densities >100 A cm^{-2} at 5 V. The turn-on voltage was 1.9–2.1 V for the heterojunction rectifiers.

Figure 5 shows the reverse I–V characteristics out to −100 V for (a) NiO/Ga_2O_3 rectifiers with 10/10 nm NiO bilayers or (b) 10/20 nm NiO bilayers. While the guard ring diameter makes little

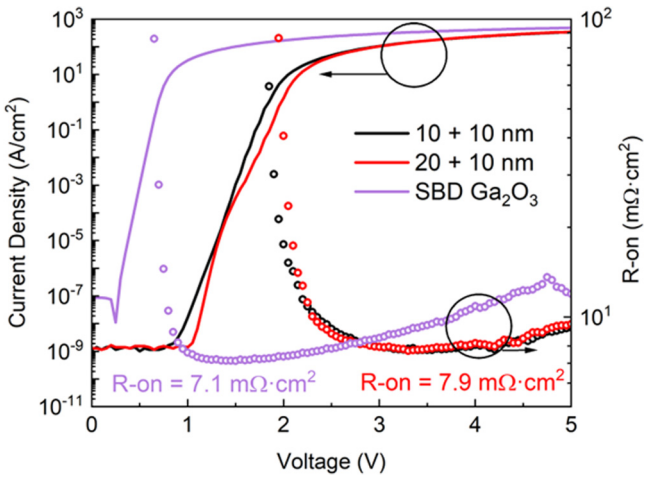

FIG. 4. Comparison of forward current density characteristics for Schottky and NiO/Ga_2O_3 rectifiers.

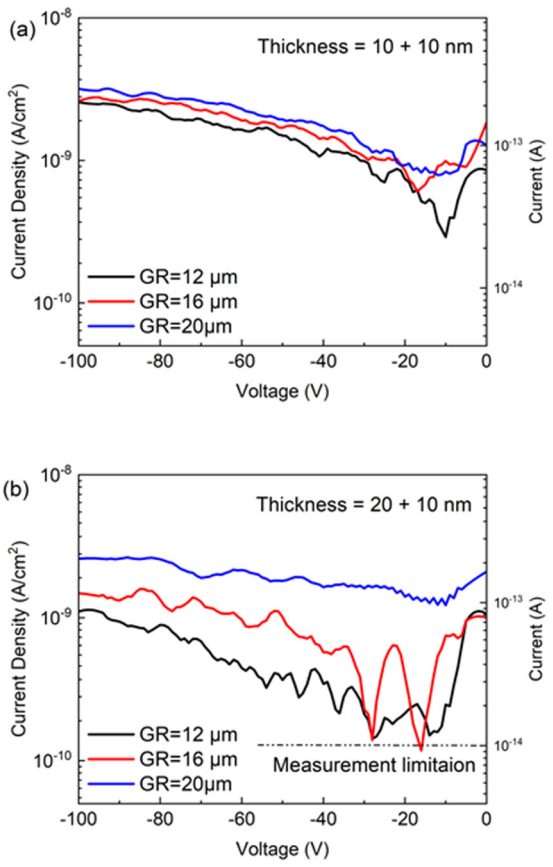

FIG. 5. Reverse I-V characteristics out to −100 V for (a) NiO/Ga_2O_3 rectifiers with 10/10 nm NiO bilayers or (b) 10/20 nm NiO bilayers.

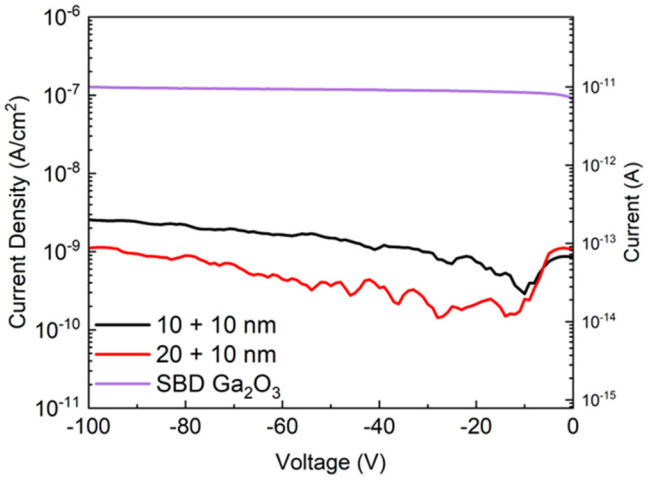

FIG. 6. Comparison of low bias reverse current characteristics between Schottky rectifiers and NiO/Ga_2O_3 rectifiers with either 10/10 nm or 10/20 nm bilayers. All these were fabricated on the sample with drift layer doping of 6.7×10^{15} cm^{-3}.

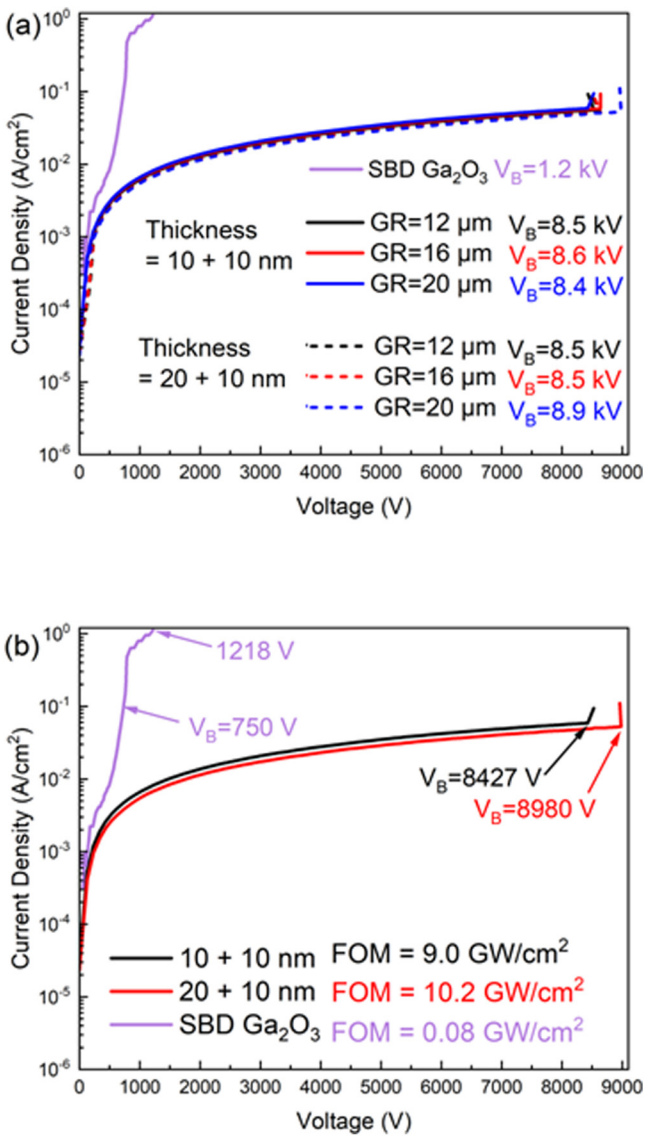

FIG. 7. (a) Reverse current characteristics from the Schottky rectifier and NiO/Ga_2O_3 heterojunction rectifiers with different guard ring extensions and NiO layer thicknesses. (b) Comparison between Schottky and NiO/Ga_2O_3 heterojunction rectifiers fabricated on the lowest drift layer doping wafer.

difference to devices with the 10/10 nm NiO bilayer, there is a reduction in reverse current density for the smaller guard rings. A comparison of the heterojunction results with those from the Schottky rectifiers all fabricated on the lower drift layer doping structure is shown in Fig. 6 for a fixed guard ring diameter of 12 μm in the latter type of device. As expected, the leakage current from the heterojunction rectifiers is lower than that of the Schottky rectifier and reducing the doping in the drift layer also lowers the reverse current density.[20,21,47–50] Similar trends were observed for the two types of devices fabricated on the higher drift layer doping. The p-n junction has a larger effective barrier for current transport than the metal gate Schottky rectifiers.

The reverse J–V characteristics over the full bias range are shown in Fig. 7(a) for the devices fabricated on the 6.7×10^{15} cm^{-3} drift layers with different NiO thicknesses as well as different guard ring diameters. Once again, for comparison, we show the result for the Schottky rectifier and for a heterojunction device fabricated ion the wafer with larger drift layer concentration of 8×10^{15} cm^{-3}. The key points from these data are first, that the lower doping produces a higher reverse breakdown voltage, with a maximum of 8.9 kV. This is the highest reported to data for Ga_2O_3 rectifiers of any type.[12] The second point is that the heterojunction really increases reverse breakdown voltage compared to the Schottky rectifier. V_b of the latter was 750 V, while the device reached 1218 V before permanent burn out. The final point is that the NiO thickness and guard ring extension length made only a relatively small difference in V_B.

Figure 7(b) shows a comparison of the breakdown voltages for the devices fabricated on the lower drift layer doped layers, as a function of the NiO thickness. The power figure of merit was 10.2 GW cm^{-2} for the optimized heterojunction rectifier, compared to 0.08 GW/cm^{-2} for the Schottky rectifier. The theoretical maximum is ~34 GW cm^{-2}, showing that further improvement should be possible as the edge termination and epi layer quality continue to evolve.[4,12] The average electric field strength is 8.7 MV/cm. For biases >100 V, the reverse leakage current follows a $\ln(I) \propto V$ relation. This indicates the dominant leakage mechanism is electron variable-range-hopping via defect-related states in the drift region.[10,12] This has been reported in detail by numerous groups.[9,10,12,14]

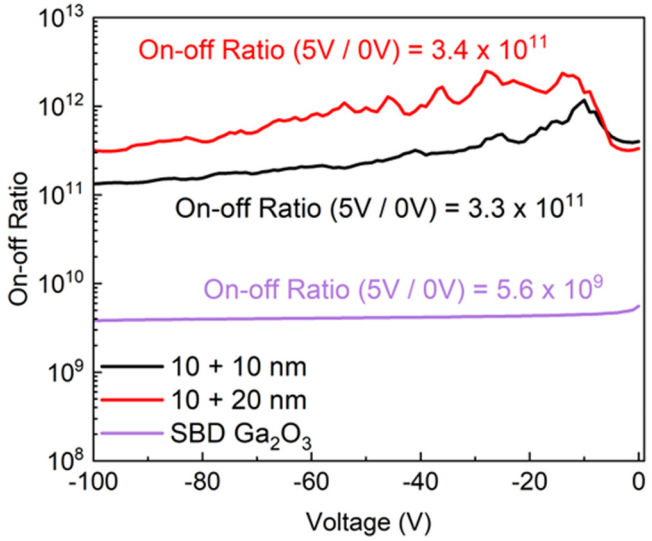

FIG. 8. On-off ratio of 100 μm diameter NiO/Ga_2O_3 heterojunction rectifiers in which the bias was switched from 5 V forward to the voltage shown on the x axis. For comparison, the results for a Schottky rectifier fabricated on the same wafer are included.

Figure 8 shows the on-off ratio of NiO/Ga_2O_3 heterojunction rectifiers in which the bias was switched from 5 V forward to the reverse voltage shown on the x axis. For comparison, the results for s Schottky rectifier fabricated on the same wafer are included. The values are still $>10^{11}$ when switching to 100 V and approximately two orders of magnitude higher than that of the Schottky rectifier over this bias range. This again emphasizes an advantage of the p-n heterojunction in achieving excellent rectification characteristics.

Figure 9 shows the reverse recovery switching waveform when switching from 50 mA forward current to −10 V for heterojunction rectifiers with (a) 10/10 nm or (b) 10/20 nm bilayers as a function of guard ring extension. The reverse recovery times are~ 21 ns and are tabulated in Table I. These measurements were made with a custom switching circuit, as described previously.[40–42] We used di/dt values around 2.9 A/μs. Others have reported use of values in the range 100–400 A/μs.[47,51] Figure 10 shows a comparison of switching waveforms of Schottky and NiO/Ga_2O_3 heterojunction rectifiers. The relative indifference to device structure demonstrates that charge storage in the p-n junction is not a significant factor compared to the Schottky device.[13,14] The Schottky diode had higher forward current due to lower effective barrier height.

Figure 11 shows a literature compilation of Ron versus V_B results for all the common types of rectifiers fabricated in the Ga_2O_3 materials system. These include metal gate Schottky barrier or junction barrier Schottky rectifiers, along with NiO/Ga_2O_3 heterojunction rectifiers. This is a standard chart for showing the improvement in Ga_2O_3 rectifier performance and contains the theoretical lines for SiC, GaN, and Ga_2O_3 devices. Note that there are now at least five instances of Ga_2O_3 rectifiers with performance beyond the one-dimensional unipolar limits of GaN and SiC. It is

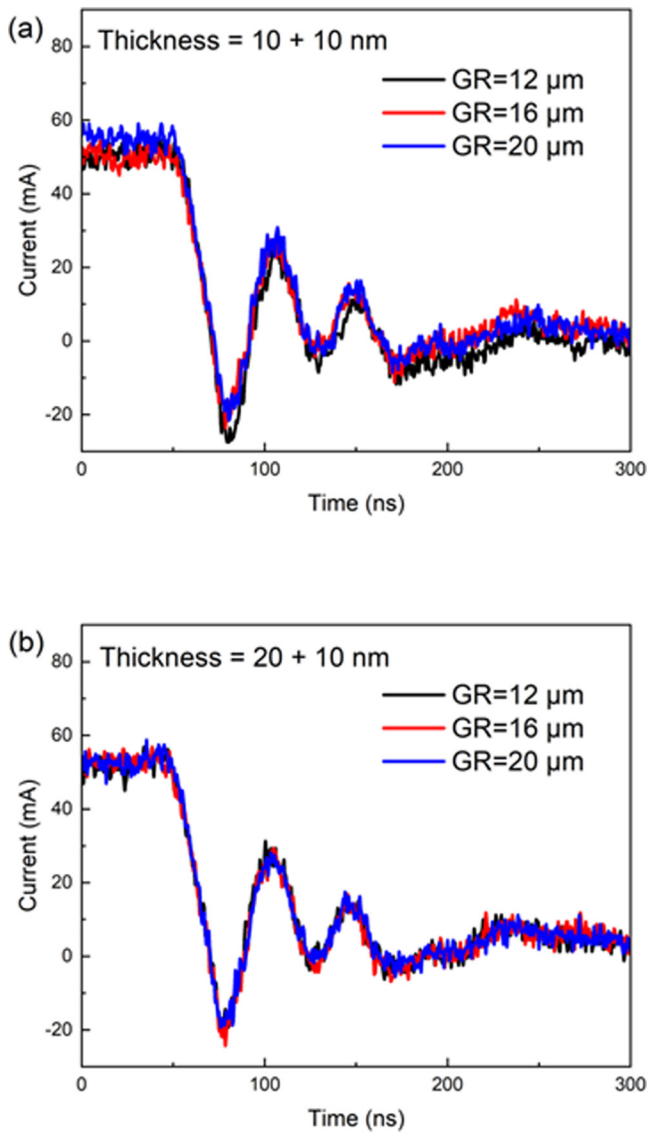

FIG. 9. (a) Switching waveform for NiO/Ga_2O_3 heterojunction rectifiers with (a) 10/10 nm or (b) 10/20 nm bilayers as a function of guard ring extension.

expected that continued optimization of the edge termination techniques and reductions in both drift layer doping and defect density should advance the ability to make large area rectifiers with high conduction currents using the NiO/Ga_2O_3 structures. The reliability of such structures will also need to be investigated.[52–54]

B. Large area devices to achieve high forward current

There has been much less reported on large area Ga_2O_3 rectifiers, which are needed to achieve large absolute forward conduction currents.[46,51,55–63] These are typically referred to as

TABLE I. Summary of reverse recovery parameters for heterojunction and Schottky rectifiers.

	T_{rr} (ns)	I_{rr} (mA)	dI/dT (A/μs)	I_F (mA)
10 + 10 nm	19.6	27.5	2.9	50
20 + 10 nm	13.8	21.6	2.9	50
Schottky	14.6	21.4	2.5	65

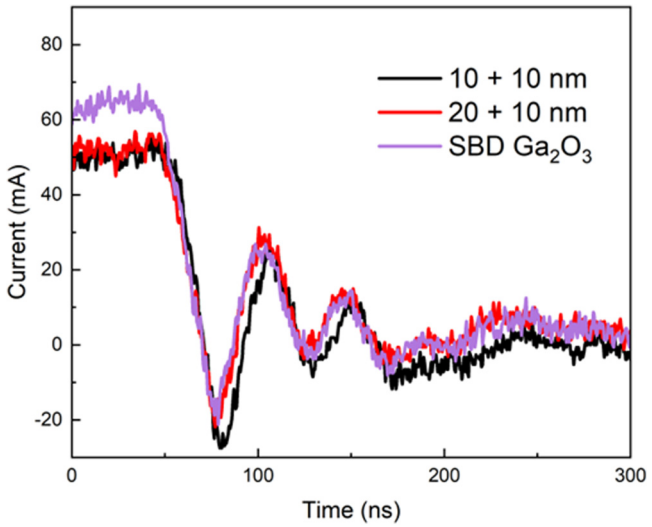

FIG. 10. Comparison of switching waveforms of Schottky and NiO/Ga_2O_3 heterojunction rectifiers.

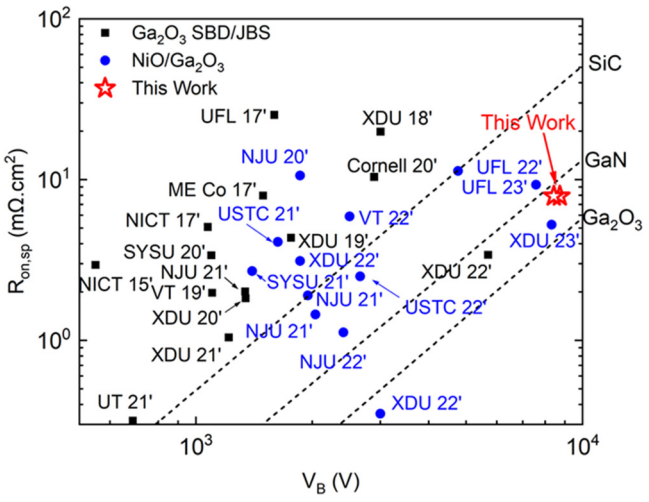

FIG. 11. Compilation of Ron vs V_B of conventional and NiO/Ga_2O_3 heterojunction small area rectifiers reported in the literature.

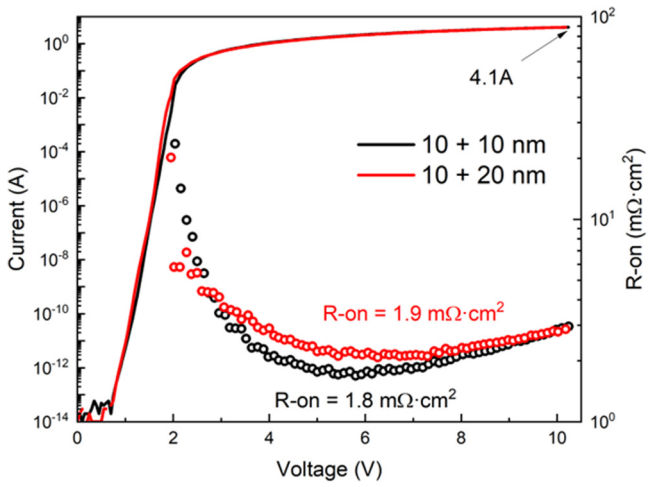

FIG. 12. Forward current characteristics for 1 mm^2 heterojunction rectifiers for two different NiO thicknesses.

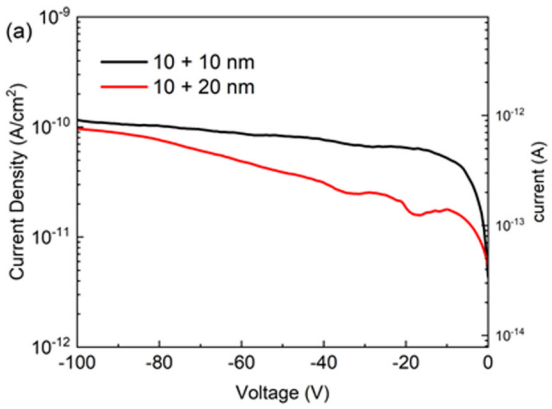

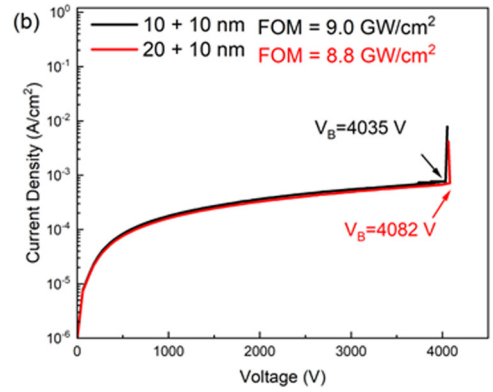

FIG. 13. Reverse J-V characteristics out to (a) −100 V for NiO/Ga_2O_3 rectifiers with 10/10 nm 10/20 nm NiO bilayers. (b) Over full bias range to show V_B.

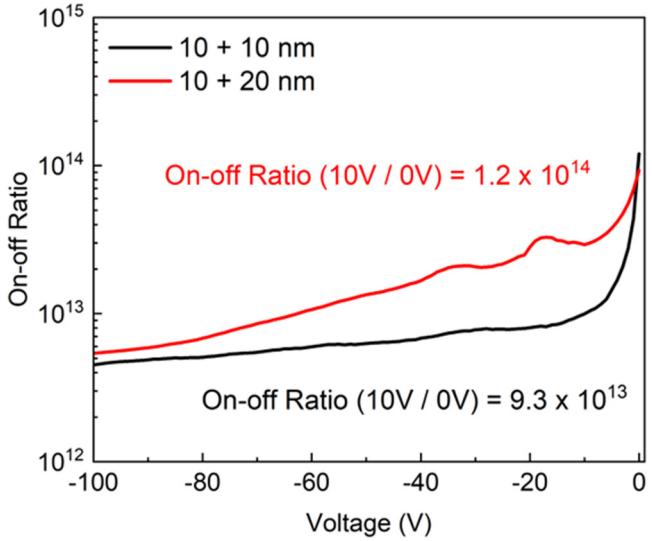

FIG. 14. On-off ratio of 1 mm^2 NiO/Ga_2O_3 heterojunction rectifiers in which the bias was switched from 5 V forward to the voltage shown on the x axis.

Ampere-class power devices. A recent review has discussed switching performance, packaging, and approaches to thermal management.[46]

We fabricated 1 mm^2 devices with the same structure as shown in Fig. 1. Figure 12 shows the forward J–V characteristics of two such devices with different NiO thicknesses, with a maximum forward current of 4.1A at 10 V forward bias. The R_{ON} values are 1.8–1.9 mΩ cm^{-2}. While rectifier arrays have achieved currents in the range of 33–100 A, 4 A for an individual device is still behind

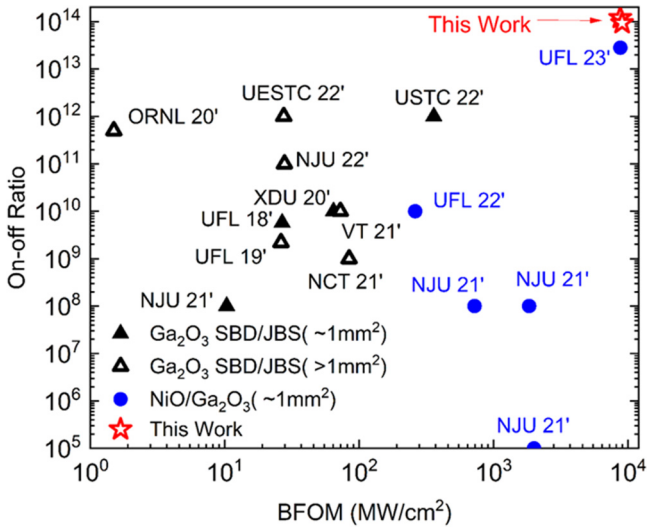

FIG. 15. Compilation of on-off ratio vs power figure of merit of conventional and NiO/Ga_2O_3 heterojunction rectifiers reported in the literature.

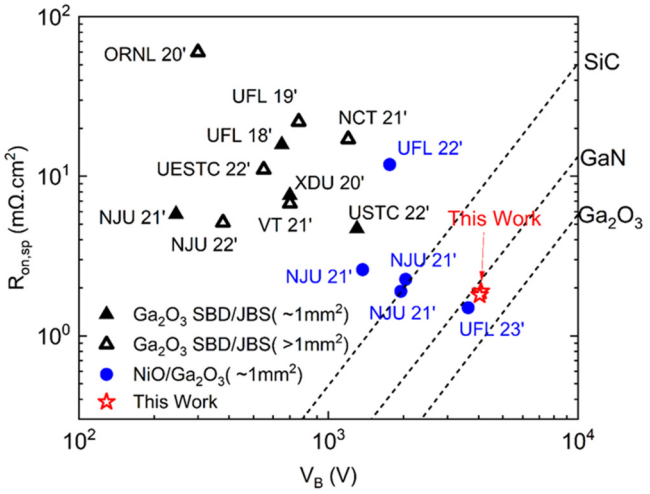

FIG. 16. Compilation of Ron vs V_B of large area conventional and NiO/Ga_2O_3 heterojunction rectifiers reported in the literature.

those of Gong *et al.*[47] and Zhou *et al.*,[51] where 12 A was achieved. Large area packaged Ga_2O_3 SBDs with an anode size of 3 × 3 mm^2 have been reported with forward current of over 15 A.[55]

The reverse J–V characteristics are shown in Fig. 13 for two different types of structure with varying NiO thickness. Figure 13 (a) shows the low voltage (−100 V) range, while (b) shows that the V_B values are around 4 kV. These are the highest reported for Ampere-class Ga_2O_3 rectifiers. Once again, the NiO thickness does not have a significant impact on the magnitude of the breakdown voltage.

Figure 14 shows the on-off ratio of 1 mm^2 NiO/Ga_2O_3 heterojunction rectifiers in which the bias was switched from 5 V forward to the voltage shown on the x axis. The on-off ratio is >10^{12} over the whole bias range investigated and is slightly better for the thicker NiO layers. For switching from 10 to 0 V, the ratio is ~10^{14} in both cases and these large area devices retain excellent rectification, showing that the increased likelihood of having defects within the active area have not degraded this property. Sdoeung *et al.*[64] reported that threading dislocations in HVPE layers of the type we are using are responsible for significant contributions to reverse leakage current in rectifiers. Figure 15 shows a compilation of on-off ratio versus power figure of merit of conventional and NiO/Ga_2O_3 heterojunction rectifiers reported in the literature.

Figure 16 shows a compilation of Ron versus V_B of large area conventional and NiO/Ga_2O_3 heterojunction rectifiers reported in the literature. Our results represent the best combination of breakdown voltage and on-state resistance reported to date and show the impressive advances in material quality in terms of reducing both background carrier density and extended defect density.

IV. SUMMARY AND CONCLUSIONS

In summary, we optimized the NiO bilayer thickness and extension of these layers beyond the cathode contact on

NiO/β-Ga_2O_3 p-n heterojunction rectifiers to achieve V_B 8.9 kV with R_{on} of 7.9 m Ω cm^2 and a resultant figure-of-merit (V_b^2/R_{on}) of 10.2 GW cm^{-2}. The heterojunction produces breakdown voltages far more than Schottky rectifiers fabricated on the same wafer and confirms that the NiO can act as both p-layer and guard ring material. This approach now consistently produces power figure of merits that exceed the unipolar power device performance of both GaN and SiC. It will still be necessary to establish the long-term reliability of devices fabricated by this approach. For large area devices, the low thermal conductivity limitations of Ga_2O_3 remain as a primary issue. In addition, more work is needed to understand the surge current capability of Ga_2O_3-based rectifiers and the packaging approaches needed to achieve practical operating characteristics, along with establishing the junction-to-ambient thermal resistance of junction side cooling approaches.[65,66]

ACKNOWLEDGMENTS

The work at UF was performed as part of Interaction of Ionizing Radiation with Matter University Research Alliance (IIRM-URA), sponsored by the Department of the Defense, Defense Threat Reduction Agency under Award No. HDTRA1-20-2-0002. The content of the information does not necessarily reflect the position or the policy of the federal government, and no official endorsement should be inferred. The work at UF was also supported by NSF DMR 1856662.

AUTHOR DECLARATIONS

Conflict of Interest

The authors have no conflicts to disclose.

Author Contributions

Jian-Sian Li: Data curation (equal); Formal analysis (equal); Investigation (equal); Methodology (equal); Writing – original draft (equal). **Chao-Ching Chiang:** Data curation (equal); Investigation (equal); Methodology (equal); Writing – original draft (equal). **Xinyi Xia:** Conceptualization (equal); Data curation (equal); Investigation (equal); Methodology (equal); Writing – original draft (equal). **Hsiao-Hsuan Wan:** Data curation (equal); Investigation (equal); Methodology (equal); Writing – original draft (equal). **Fan Ren:** Conceptualization (equal); Data curation (equal); Formal analysis (equal); Funding acquisition (equal); Investigation (equal); Methodology (equal); Project administration (equal); Writing – original draft (equal). **S. J. Pearton:** Conceptualization (equal); Data curation (equal); Formal analysis (equal); Funding acquisition (equal); Writing – original draft (equal).

DATA AVAILABILITY

The data that support the findings of this study are available within the article.

REFERENCES

[1]M. H. Wong and M. Higashiwaki, IEEE Trans. Electron Devices **67**, 3925 (2020).
[2]X. Lu, Y. X. Deng, Y. L. Pei, Z. M. Chen, and G. Wang, J. Semicond. **44**, 061802 (2023).
[3]Andrew J. Green *et al.*, APL Mater. **10**, 029201 (2022).
[4]S. J. Pearton, Fan Ren, Marko Tadjer, and Jihyun Kim, J. Appl. Phys. **124**, 220901 (2018).
[5]Chenlu Wang *et al.*, J. Phys. D: Appl. Phys. **54**, 243001 (2021).
[6]Y. Kokubun, S. Kubo, and S. Nakagomi, Appl. Phys. Express **9**, 091101 (2016).
[7]Yuxin Deng *et al.*, Appl. Surf. Sci. **622**, 156917 (2023).
[8]Maria Isabel Pintor-Monroy, Diego Barrera, Bayron L. Murillo-Borjas, Francisco Javier Ochoa-Estrella, Julia W. P. Hsu, and Manuel A. Quevedo-Lopez, ACS Appl. Mater. Interfaces **10**, 38159 (2018).
[9]Xinyi Xia, Jian-Sian Li, Chao-Ching Chiang, Timothy Jinsoo Yoo, Fan Ren, Honggyu Kim, and S. J. Pearton, J. Phys. D: Appl. Phys. **55**, 385105 (2022).
[10]Hehe Gong, Xuanhu Chen, Yang Xu, Yanting Chen, Fangfang Ren, Bin Liu, Shulin Gu, Rong Zhang, and Jiandong Ye, IEEE Trans. Electron Devices **67**, 3341 (2020).
[11]S. Sharma, K. Zeng, S. Saha, and U. Singisetti, IEEE Electron Device Lett. **41**, 836 (2020).
[12]Jincheng Zhang *et al.*, Nat. Commun. **13**, 3900 (2022).
[13]Pengfei Dong, Jincheng Zhang, Qinglong Yan, Zhihong Liu, Peijun Ma, Hong Zhou, and Yue Hao, IEEE Electron Device Lett. **43**, 765 (2022).
[14]Jian-Sian Li, Chao-Ching Chiang, Xinyi Xia, Timothy Jinsoo Yoo, Fan Ren, Honggyu Kim, and S. J. Pearton, Appl. Phys. Lett. **121**, 042105 (2022).
[15]S. Roy, A. Bhattacharyya, P. Ranga, H. Splawn, J. Leach, and S. Krishnamoorthy, IEEE Electron Device Lett. **42**, 1140 (2021).
[16]Arkka Bhattacharyya *et al.*, Appl. Phys. Express **15**, 061001 (2022).
[17]Kevin. D. Chabak *et al.*, Semicond. Sci. Technol. **35**, 013002 (2020).
[18]Zongyang Hu *et al.*, Appl. Phys. Lett. **113**, 122103 (2018).
[19]Ribhu Sharma, Minghan Xian, Chaker Fares, Mark E. Law, Marko Tadjer, Karl D. Hobart, Fan Ren, and Stephen J. Pearton, J. Vac. Sci. Technol. A **39**, 013406 (2021).
[20]Wenshen Li, Devansh Saraswat, Yaoyao Long, Kazuki Nomoto, Debdeep Jena, and Huili Grace Xing, Appl. Phys. Lett. **116**, 192101 (2020).
[21]Y. Lv *et al.*, IEEE Trans. Power Electron. **36**, 6179 (2021).
[22]C. Liao *et al.*, IEEE Trans. Electron Devices **69**, 5722 (2022).
[23]Ming Xiao *et al.*, IEEE Trans. Power Electron. **36**, 8565 (2021).
[24]X. Lu, Xianda Zhou, Huaxing Jiang, Kar Wei Ng, Zimin Chen, Yanli Pei, Kei May Lau, and Gang Wang, IEEE Electron Device Lett. **41**, 449 (2020).
[25]Chenlu Wang *et al.*, IEEE Electron Device Lett. **42**, 485 (2021).
[26]Qinglong Yan *et al.*, Appl. Phys. Lett. **118**, 122102 (2021).
[27]H. H. Gong, X. H. Chen, Y. Xu, F.-F. Ren, S. L. Gu, and J. D. Ye, Appl. Phys. Lett. **117**, 022104 (2020).
[28]Hehe Gong *et al.*, IEEE Trans. Power Electron. **36**, 12213 (2021).
[29]H. H. Gong *et al.*, Appl. Phys. Lett. **118**, 202102 (2021).
[30]W. Hao *et al.*, Appl. Phys. Lett. **118**, 043501 (2021).
[31]F. Zhou *et al.*, IEEE Trans. Power Electron. **37**, 1223 (2022).
[32]Qinglong Yan *et al.*, Appl. Phys. Lett. **120**, 092106 (2022).
[33]Jian Sian Li, Hsiao Hsuan Wan, Chao Ching Chiang, Xinyi Xia, Timothy Yoo, Honggyu Kim, Fan Ren, and S. J. Pearton, Crystals **13**, 886 (2023).
[34]Jiaye Zhang *et al.*, ACS Appl. Electron. Mater. **2**, 456 (2020).
[35]Yuangang Wang *et al.*, IEEE Trans. Power Electron. **37**, 3743 (2022).
[36]Hong Zhou, Shifan Zeng, Jincheng Zhang, Zhihong Liu, Qian Feng, Shengrui Xu, Jinfeng Zhang, and Yue Hao, Crystals **11**, 1186 (2021).
[37]Zhengpeng Wang *et al.*, IEEE Trans. Electron Devices **69**, 981 (2022).
[38]Boyan Wang, Ming Xiao, Joseph Spencer, Yuan Qin, Kohei Sasaki, Marko J. Tadjer, and Yuhao Zhang, IEEE Electron Device Lett. **44**, 221 (2023).
[39]F. Zhou *et al.*, Appl. Phys. Lett. **119**, 262103 (2021).
[40]J. Yang, F. Ren, Y.-T. Chen, Y.-T. Liao, C.-W. Chang, J. Lin, M. J. Tadjer, S. J. Pearton, and A. Kuramata, IEEE J. Electron Devices Soc. **7**, 57 (2019).
[41]Yen-Ting Chen, Jiancheng Yang, Fan Ren, Chin-Wei Chang, Jenshan Lin, S. J. Pearton, Marko J Tadjer, Akito Kuramata, and Yu-Te Liao, ECS J. Solid State Sci. Technol. **8**, Q3229 (2019).

[42]Jian-Sian Li, Chao-Ching Chiang, Xinyi Xia, Fan Ren, and S. J. Pearton, J. Vac. Sci. Technol. A **40**, 063407 (2022).
[43]W. Hao, Q. He, X. Zhou, X. Zhao, G. Xu, and S. Long, *2022 IEEE 34th International Symposium on Power Semiconductor Devices and ICs (ISPSD)*, Vancouver, BC, Canada, September 2022 (IEEE, New York, 2022), pp. 105–108.
[44]Weibing Hao *et al.*, *2022 International Electron Devices Meeting (IEDM)*, San Francisco, CA, December 2022 (IEEE, New York, 2022), pp. 9.5.1–9.5.4.
[45]X. Zhou, Q. Liu, W. Hao, G. Xu, and S. Long, *2022 IEEE 34th International Symposium on Power Semiconductor Devices and ICs (ISPSD)*, Vancouver, BC, October 2022 (IEEE, New York, 2022), pp. 101–104.
[46]Yuan Qin, Zhengpeng Wang, Kohei Sasaki, Jiandong Ye, and Yuhao Zhang, Jpn. J. Appl. Phys. **62**, SF0801 (2023).
[47]Zhengpeng Wang *et al.*, IEEE Trans. Electron Devices **69**, 981 (2022).
[48]J. Yang, F. Ren, M. Tadjer, S. J. Pearton, and A. Kuramata, AIP Adv. **8**, 055026 (2018).
[49]J. Yang, C. Fares, R. Elhassani, M. Xian, F. Ren, S. J. Pearton, M. Tadjer, and A. Kuramata, ECS J. Solid State Sci. Technol. **8**, Q3159 (2019).
[50]M. Ji, N. R. Taylor, I. Kravchenko, P. Joshi, T. Aytug, L. R. Cao, and M. P. Paranthaman, IEEE Trans. Power Electron. **36**, 41 (2021).
[51]Hehe Gong, Feng Zhou, Xinxin Yu, Weizong Xu, Fang-Fang Ren, Shulin Gu, Hai Lu, Jiandong Ye, and Rong Zhang, IEEE Electron Device Lett. **43**, 773 (2022).
[52]Zahabul Islam, Aman Haque, Nicholas Glavin, Minghan Xian, Fan Ren, Alexander Y. Polyakov, Anastasia Kochkova, Marko Tadjer, and S. J. Pearton, ECS J. Solid State Sci. Technol. **9**, 055008 (2020).
[53]Z. Islam, M. Xian, A. Haque, F. Ren, M. Tadjer, and S. J. Pearton, IEEE Trans. Electron Devices **67**, 3056 (2020).
[54]Rujun Sun, Andrew R. Balog, Haobo Yang, Nasim Alem, and Michael A. Scarpulla, IEEE Electron Device Lett. **44**, 725 (2023).
[55]B. Wang, Ming Xiao, Zichen Zhang, Yifan Wang, Yuan Qin, Qihao Song, Guo-Quan Lu, Khai Ngo, and Yuhao Zhang, IEEE Trans. Electron Devices **70**, 633 (2023).
[56]H. Gong, F. Zhou, X. Yu, W. Xu, F. Ren, S. Gu, H. Lu, J. Ye, and R. Zhang, IEEE Electron Device Lett. **43**, 773 (2022).
[57]F. Otsuka, H. Miyamoto, A. Takatsuka, S. Kunori, K. Sasaki, and A. Kuramata, Appl. Phys. Express **15**, 016501 (2022).
[58]Jiancheng Yang *et al.*, Appl. Phys. Lett. **114**, 232106 (2019).
[59]Xinyi Xia, Jian-Sian Li, Chao-Ching Chiang, Fan Ren, and Stephen J. Pearton, ECS Trans. **111**, 103 (2023).
[60]Y. Lv *et al.*, IEEE Trans. Power Electron. **36**, 6179 (2021).
[61]J. Wei, Y. Wei, J. Lu, X. Peng, Z. Jiang, K. Yang, and X. Luo, *2022 IEEE 34th International Symposium on Power Semiconductor Devices and ICs (ISPSD)* Toronto, Canada. May 2022 (IEEE, New York, 2022), pp. 97–100.
[62]W. Hao *et al.*, IEEE Trans. Electron Devices **70**, 2129 (2023).
[63]J.-S. Li, C.-C. Chiang, X. Xia, C.-T. Tsai, F. Ren, Y.-T. Liao, and S. J. Pearton, ECS J. Solid State Sci. Techol. **11**, 105003 (2022).
[64]Sayleap Sdoeung, Kohei Sasaki, Katsumi Kawasaki, Jun Hirabayashi, Akito Kuramata, and Makoto Kasu, Jpn. J. Appl. Phys. **62**, SF1001 (2023).
[65]B. Wang, Ming Xiao, Jack Knoll, Cyril Buttay, Kohei Sasaki, Christina Dimarino, and Yuhao Zhang, IEEE Electron Device Lett. **42**, 1132 (2021).
[66]Jian Sian Li, Chao Ching Chiang, Xinyi Xia, Hsia Hsuan Wan, Fan Ren, and S. J. Pearton, "Superior high temperature performance of 8 kV NiO/Ga_2O_3 vertical heterojunction rectifiers," J. Mater. Chem. C (to be published) (2023).